X-953-77-27
PREPRINT

TMX - 71296

A REVIEW OF APPLICATIONS OF MICROWAVE RADIOMETRY TO OCEANOGRAPHY

(NASA-TM-X-71296) A REVIEW OF APPLICATIONS OF MICROWAVE RADIOMETRY TO OCEANOGRAPHY (NASA) 22 p HC A02/MF A01 CSCL 08C
N77-21818
Unclas
G3/48 25820

THOMAS T. WILHEIT, JR.

FEBRUARY 1977

GSFC
GODDARD SPACE FLIGHT CENTER
GREENBELT, MARYLAND

1

X-953-77-27
Preprint

A REVIEW OF APPLICATIONS OF MICROWAVE RADIOMETRY TO OCEANOGRAPHY

Thomas T. Wilheit, Jr.

February 1977

GODDARD SPACE FLIGHT CENTER
Greenbelt, Maryland

A REVIEW OF APPLICATIONS OF MICROWAVE RADIOMETRY TO OCEANOGRAPHY

Thomas T. Wilheit, Jr.

ABSTRACT

The thermal microwave radiation from the ocean surface as seen from above the atmosphere is a function of the surface temperature and wind speed and is modified by liquid water and water vapor in the intervening atmosphere. Further, if the ocean surface is frozen, the emissivity is drastically increased and the effect of the intervening atmosphere is generally negligible. The emissivity of first year ice is somewhat larger than for multi-year ice.

Using the above physics, the data from the Electrically Scanning Microwave Radiometers (ESMR's) on the Nimbus-5 and Nimbus-6 satellites operating at wavelengths of 1.55 cm and 8 mm respectively can be interpreted in terms of rain rate, ice coverage and first year versus multi-year ice determination. The rain rate data is being used to establish a climatology of rainfall over the oceans. The ice data is being used by the United States Navy in support of international scientific efforts in the Antarctic region. Both ice and rain data sets have been generated for the Global Atmospheric Research Project Data Systems Test.

It is possible, by making multifrequency measurements, to separate the surface and atmospheric effects and to make useful measurements of sea surface temperature, surface wind speed, and atmospheric parameters along with improved measurements of rain and ice.

CONTENTS

ILLUSTRATIONS

ILLUSTRATIONS (Continued)

A REVIEW OF APPLICATIONS OF MICROWAVE RADIOMETRY TO OCEANOGRAPHY

INTRODUCTION

Recent developments, most notably the launch of microwave radiometers aboard the Nimbus-5 satellite in 1972 and the Nimbus-6 satellite in 1975, have opened the microwave portion of the electromagnetic spectrum for Earth observations. These observations have applications in many disciplines, meteorology, hydrology, and glaciology in addition to oceanography. The aim of this paper is to discuss the applications of microwave radiometry, the measurement of thermal microwave radiation, to oceanography. To this end, we will first review the essential physics of microwave radiative transfer, we will show oceanographic applications of this physics using data from the Nimbus-5 and 6 Electrically Scanned Microwave Radiometer (ESMR's) and examine future applications expected from the Scanning Multifrequency Microwave Radiometer (SMMR) which is presently scheduled to be launched on both the Nimbus-G and Seasat-A satellites in 1978. Although it is, perhaps, the most dramatic of the oceanographic applications of microwave radiometry, the mapping of sea ice will not be treated in depth here becuase two companion papers discuss this application in some detail.

The microwave region for the purpose of this paper will be considered to be from about 1 GHz (30 cm) to 40 GHz (7.5 mm). At frequencies below about 1 GHz the practical difficulties of making measurements (radio frequency interference, galactic background noise, resolution) make extensive oceanographic application improbable and above 40 GHz atmospheric opacity makes measurements more pertinent to meteorology than to oceanography. Because the wavelengths involved here are significant when compared with the size of instruments that might reasonably be placed on aircraft or spacecraft platforms, diffraction is the principal limitation to resolution. This limits the angular resolution (angular separation between half of maximum power points) to approximately

$$\Delta\theta \cong 1.2\,\lambda/D \tag{1}$$

where $\Delta\theta$ is the beamwidth in radians, λ is the wavelength and D is the width of the aperture projected on a plane normal to the direction of view. The factor of 1.2 is approximate and varies somewhat in practice. The Nimbus-5 ESMR provides a typical example. Its aperture is a square about 80 cm on each side, the operating wavelength is 1.55 cm and it views the Earth from about 1100 km altitude. The resultant resolution is 25 km when viewing directly at nadir (normal to aperture). The Nimbus-5 and 6 ESMR's have been discussed in detail by Wilheit (1972 and 1975).

BACKGROUND PHYSICS

Because of the validity of the Rayleigh Jeans approximation in the microwave region, the law of radiative transfer may be expressed quite simply

$$\frac{dT_B}{dx} = -\gamma\,(T_B - t_0) \tag{2}$$

where T_B is the microwave radiance expressed as an equivalent black body temperature, γ is the absorption coefficient at the point x and t_0 is the thermodynamic temperature of the medium at that point. The derivative is along the direction of propagation. It must be emphasized that γ is only the attenuation due to loss mechanisms; scattering and reflection must be accounted for by appropriate re-distribution of radiation among directions of propagation.

A typical Earth viewing geometry is shown in Figure 1. In order to calculate the brightness temperature expected for such a situation, one first divides the atmosphere up into a number of layers each of which may be characterized by a uniform temperature and absorption coefficient. Beginning with the 3° K cosmic background, the radiation is then propagated from the top downwards through each layer according to Equation 2. A fraction R (the reflectivity) is reflected from the surface and the surface also radiates an amount Et where E is a quantity characteristic of the surface, the emissivity, having a value between 0 and 1 and t is the thermodynamic temperature of the surface. Arguments based on thermodynamic equilibruim show that E and R are related by:

$$E + R = 1 \tag{3}$$

Since water is a polar molecule it has a very large dielectric constant at microwave frequencies. This results in a large reflectivity (low emissivity) for a liquid water surface such as the ocean. In Figure 2, the emissivity is calculated for a smooth water surface using the dielectric constant data for 20° C of Lane and Saxton (1952) and the Fresnel relations (Jackson 1962). Note that the emissivity increases somewhat with frequency over the range, and that for viewing at an oblique angle the horizontal polarization yields a lower and vertical a higher emissivity than that for nadir viewing where the distinction between the two polarizations breaks down. The emissivity was calculated both for fresh water and for a 3.5% NaCl solution which is a reasonable approximation to sea water; there is no consequential difference between fresh and sea water except at the very low frequency end of the spectrum, below about 5 GHz. Since most solid surfaces have emissivity in the range 0.8 to 0.95 and 0.5 is a typical value for water, there is a striking contrast between liquid water surfaces such as lakes, rivers, and the oceans and solid surface such as land and sea ice. This low emissivity of the sea surface also provides a good background for viewing the intervening atmosphere.

The emissivities shown in Figure 2 were calculated for a smooth water surface. However, when the wind blows across the surface of the ocean, it generates roughness and foam. The effect of roughness on the emissivity of the water surface depends strongly on the viewing angle and polarization. For viewing directly at nadir where the distinction between vertical and horizontal polarizations disappears, roughness has very little effect on emissivity; for viewing in horizontal polarization at angles away from nadir the roughness increases the emissivity and for vertical polarization for view angles between 0° (nadir) and 55° the roughness increases the emissivity while it decreases the emissivity for view angles greater than about 55°, as was determined experimentally by Hollinger (1972). Foam cover, on the other hand, always increases the emissivity of the surface. Figure 3 shows the increase in brightness temperature caused by a given wind speed as found by Nordberg et al. (1971) for a frequency of 19.35 GHz and for nadir viewing. They found no effect, in their case, for wind speeds less than 7 m/s and an increase of around 1° Ks/m above that. This relationship has been investigated further by Webster et al. (1975). They examined a frequency range of from 1.4 to 37 GHz and a view angle of 38° (both polarizations). Figure 4 summarizes their results. Here the rate of increase of brightness temperature with increasing wind speed is shown for all frequencies observed. Note first that viewing in horizontal polarization enhances and viewing in vertical polarization decreases the strength of the effect vis-a-vis nadir viewing. This is because in horizontal polarization the effect of roughness and of foam both increase with increasing wind speed and because viewing in horizontal polarization decreases the emissivity of the undisturbed surface thereby increasing the emissivity contrast between the foam and open water with respect to nadir viewing. The converse argument for foam and the relative weakness of the roughness effect account for the vertical polarization case. Note also that the spectrum of the net effect is only weakly frequency dependent above about 10 GHz but it decreases somewhat at lower frequencies.

The temperature of the sea surface also effects its emissivity. In Figure 5, the change in sea surface emission (emissivity times temperature) per change in temperature over the range of 0 to 30° C is shown as a function of frequency for nadir viewing and for vertical polarization at a 50° view angle. Note that there is a broad maximum near 5 GHz and nulls near 1.5 and 20 GHz. At the null points, the emissivity is inversely proportional to the absolute temperature and thus the product is independent of temperature. Below 1.4 GHz and above 20 GHz the emissivity change overpowers the temperature change so that an increase in temperature actually decreases the net emission.

In contrast to the low emissivity of the open ocean, sea ice has a rather high emissivity (ca. 0.85). This results in a large increase in the emission from the sea surface when it freezes. Further, two different categories of sea ice may be distinguished from their microwave emissivities. Wilheit et al. (1971) identified these two types of ice as old and new based on photographic and laser profilometer data. Gloersen et al. (1973) further defined the categories as being first-year and multi-year ice based on direct in situ observations of the ice. Figure 6 shows the emissivity of both types of ice as a function of frequency. First year ice has a emissivity of 0.95 over the entire observed range (5 to 37 GHz) whereas the multi-year ice emissivity decreases with increasing frequency.

For present purposes, the atmosphere consists of three constituents, molecular oxygen, water vapor and liquid water droplets. Ice, as in cirrus clouds, is not a significant factor in the microwave frequency range. Molecular oxygen has a series of resonances in the 50 to 70 GHz range which at sea level pressure merge to form a band of absorption which makes quantitative determination of surface properties difficult or impossible between about 40 to 80 GHz. In Figure 7, the absorption due to water vapor (Staelin, 1966) is shown for the United States Standard Atmosphere. There is a single rather weak line at 22.235 GHz which has a half width of about 1 GHz at sea level due to pressure broadening; there are also a number of very strong lines at 183 GHz and higher. The increase in absorption noted above 31 GHz is due to the influence of the far wings of these lines.

For water droplets, two cases must be considered, raining and non-raining. In the non-raining case, the small droplet (Rayleigh) limit is applicable (Gunn and East, 1954) and the net absorption coefficient becomes proportional to the net density of liquid water independent of the droplet size distribution as long as there are no particles larger than about 100μm. A typical status cloud containing 20 mg/cm^2 of liquid water would have an optical depth of about 10^{-3} at 5 GHz and would vary approximately as the frequency squared.

As larger and larger drops are considered, the absorption coefficient is first increased over the Rayleigh approximation as the dropsize becomes comparable to the wavelength and then decreases below the Rayleigh approximation due to screening of the interior of the drop. Also, as the dropsize increases scattering becomes significant. Thus, since a rain cloud contains more water and larger drops than a non-raining cloud, it has greatly enhanced microwave absorption. In Figure 8, the total extinction (scattering plus absorption) and scattering coefficients calculated for a frequency of 19.35 GHz as a function of rain rate for a Marshall-Palmer dropsize distribution are shown (Wilheit <u>et al.</u>, 1975 II). At rainrates greater than a few mm/hr, the scattering becomes significant, greatly complicating the radiative transfer computations; a method of handling this complication is discussed by Wilheit <u>et al.</u>, (1975 II).

The combination of water vapor and water droplets prevents use of frequencies above the molecular oxygen band for quantitative surface property determination.

APPLICATIONS

1. Rainfall Intensity

In Figure 9, data from the Nimbus-5 ESMR is displayed as an image (Wilheit <u>et al.</u>, 1976). In this image, dark areas represent high brightness temperatures and light areas represent low brightness temperatures with a dynamic range from about 190° K to 250° K. The most obvious feature visible is the southeastern portion of the United States. This stands out because of the large emissivity contrast between land (ca. 0.9) and water (ca. 0.4). But, in addition to the known land features, there is a dark streak extending from the North Carolina coast, through the Atlantic Ocean and curving across Florida and continuing into the Gulf of Mexico. The microwave brightness temperature in this feature must exceed 190° K to be within the dynamic range of the image and geographically this area is known to be open ocean. If one allows for reasonable values for surface wind speed, atmospheric water vapor and non-raining clouds, it is not nearly enough to account for the observed temperatures. Rain is the only readily apparent phenomenon which would explain it. It is possible to verify that this feature does correspond to rain. Figure 10 is a summary of meteorological radar observations made within five minutes of the satellite observations. The area of rain indicated by the radar corresponds quite closely to the feature. The break in the rain area in the Atlantic Ocean is an artifact caused by the particular locations and limited range of radar stations.

It is possible to go further than simply identifying areas of rain with the Nimbus-5 ESMR data. Figure 11 shows a comparison between brightness temperature and rain rate. The black dots represent comparisons of brightness temperature as derived from the Nimbus-5 ESMR data and rain rate derived from meteorological radar and averaged over the instantaneous field of view of the ESMR. The crosses represent the results of a comparison experiment wherein a radiometer, also operating at a frequency of 19.35 GHz and viewing upward from the ground is compared with direct measurements of rain rate. The upward viewing brightness temperatures are converted into equivalent downward viewing brightness temperatures. The solid line represents a radiative transfer model of the rain which is described by Wilheit et al. (1975). The dashed line represents an envelope of a factor of two in rain rate, or 2 mm/hr, wherever is greater, about the solid line. Although there are internal inconsistencies in this model, it agrees quite well with both the space and ground based data. This effect depends on the thickness of the rain layer which is taken to be from the surface to the freezing level. For interpretation of data one must resort to climatology for this thickness which has a maximum value of about 5 km in the tropics.

This technique of measuring rainfall intensity has been applied by Rao et al. (1976) to estimate rainfall climatology over the worlds oceans. They have used Nimbus-5 ESMR data to produce weekly, monthly, seasonally, and annually averaged rainfall maps for the world's major ocean areas for December of 1972 through February 1975. As an example, in Figure 12 a portion of the Pacific Ocean is shown for two Januarys, one an El Niño year (1973) and the other (1974) not. Note that the rainfall patterns are quite different in the two years showing the gross changes in the weather patterns associated with the ocean current changes of the El Niño phenomenon.

Polar Ice Analysis

The data from the Nimbus-5 ESMR in the form of 20 x 25 cm (8 x 10 inch) black and white prints as illustrated in Figure 13 have been delivered to the United States Navy since December 1972 to aid their polar ice analysis. The independence from lightning and cloud conditions of this sensor is advantageous in the polar regions; the resolution (25 km) is a severe limitation. Nevertheless, the skill developed by the Navy analysts in interpreting these images, combined with their intimate knowledge of ice behavior in their assigned regions has enabled them to make ice boundary and concentration analyses accurate to within 10 km and one eighth of ice cover. This is significantly better than the prima facie quality of the data. Such analyses have been confirmed by ships transversing the ice pack (Lt. Cdr. T. Nelson 1975, Priv. Comm.).

An interesting feature can be noted in Figure 13, an area of open water in the Eastern Weddell Sea completely surrounded by ice. This feature has been observed in the Austral winters of 1974, 75, and 76 but was absent in the Austral winter of 1973. That this area was, indeed, ice free was confirmed by the Soviet vessel Kapitan Markhov on November 22, 1975 as it transited the area with the aid of ice information supplied by the United States Navy (Lt. Cdr. T. Nelson 1975, Priv. Comm.).

Since higher frequencies make better spatial resolution possible for a given aperture and viewing geometry, it would appear that a higher frequency than the 19.35 GHz of the Nimbus-5 ESMR would be desirable for an ice monitoring system. Interfering effects caused by variations in the atmosphere and ice surface would, on the other hand, increase with frequency. The Nimbus-6 ESMR, having an operating frequency of 37 GHz, provided an opportunity to evaluate the seriousness of the interfering effects at a higher frequency. The images from this instrument have also been provided to the Navy since the summer of 1975. The Navy analysts have found many situtations where atmospheric phenomena caused errors in deducing ice boundaries from the Nimbus-6 ESMR data while they had no such difficulty with Nimbus-5. This suggests that if a single frequency system is to be used for ice monitoring it should be lower than 37 GHz but that it, perhaps, could be somewhat higher than 19.35 GHz.

Multifrequency Radiometer Applications

In the applications discussed so far, only single frequency systems have been discussed. Since the microwave brightness temperature at any frequency depends on many geophysical variables which vary independently, it is not possible to interpret the single frequency measurements quantitatively except for instances where one effect totally dominates the remaining effects as in the case of rain and ice cover.

However, the differing spectral properties of the various constituents makes it possible to separate the contributions to the brightness temperatures by making measurements at several, well chosen, frequencies. As an example of this technique Wilheit and Fowler (1977) have deduced surface wind speeds from two different sets of airborne radiometer measurements, 10.7 and 37 GHz (dual polarized - 38° nadir angle) and 19.35, 22.235, and 31.4 GHz (nadir viewing) the effect of variation of sea surface temperature could be ignored in this case as its effect was small enough to be absorbed in the measurement uncertainties.

In general, one interprets these data by a linear matrix technique such that

$$\vec{p} = \overset{\Rightarrow}{A} \cdot \vec{d} \tag{4}$$

where $\vec{p}$ is a vector of the desired parameters $\vec{d}$ is a data vector containing brightness temperatures, functions of brightness temperatures and ancillary data. The matrix $\overset{\Rightarrow}{A}$ is generated from radiative transfer models and specific values may be chosen according to climatology, geographical position and/or approximate values of the parameters in $\vec{p}$. Different approaches to generating these matrices are discussed by Wilheit and Fowler (1976), Waters et al. (1975) and Staelin et al. (1975).

A yet to be launched system, the Scanning Multifrequency Microwave Radiometer (SMMR) is intended to make simultaneous determinations of sea surface temperature, wind speed at the sea surface, and the atmospheric content of water vapor and liquid under nearly all weather conditions. The instrument will measure brightness temperature at frequencies of 6.6, 10.7, 18, 21, and 37 GHz, both horizontal and vertical polarization at an incidence angle of 50°. Copies of the instrument are scheduled to be launched on both the Nimbus-G and Seasat-A satellites in 1978. Since all frequencies share the same aperture, the spatial resolution is proportional to wavelength varying from about 125 km at 6.6 GHz to about 25 km at 37 GHz. One way of using the data from such an instrument is as follows. When the data are calibrated and earth located, they are averaged over three different grids. All five frequencies are averaged over a 150 km grid, the four highest frequencies over a 90 km grid and the three highest over a 60 km grid. Corrections are generated for rain covering part of a given grid. The 150 km grid with its 10 brightness temperatures is interpreted for sea surface temperature and for a low resolution surface wind speed. Then this sea surface temperature is used as an additional input to the 8 brightness temperatures to extract a wind speed value with 90 km resolution; both wind speed and sea surface temperature are used as additional data on the 60 km grid to extract atmospheric water parameters at 60 km resolution. Recent numerical simulations of this system suggest accuracies of about 1.5° C in sea surface temperature and 1 m/s in wind speed (A.T.C. Chang priv. comm. 1975). Much of this error is due to the fact that we are using a linear approximation for a non-linear problem. Practical techniques for mitigating this nonlinearity are being investigated. It will, no doubt, be difficult to obtain appropriate surface truth to prove a 1 m/s wind speed accuracy.

SUMMARY

The brightness temperature observed by a microwave radiometer viewing the ocean through the atmosphere in the range 1-40 GHz is affected subtly by clouds and water vapor in the atmosphere and by the surface temperature and wind speed and strikingly by rain and the phase (liquid versus ice) of the surface. The single frequency measurements currently being made from space (Nimbus-5 and 6 ESMR's) can exploit the striking effects and the SMMR's to be flown on Nimbus-G and Seasat-A will enable separation of the more subtle effects to useful accuracies.

REFERENCES

Gloersen, P., W. Nordberg, T. J. Schmugge, T. T. Wilheit, and W. J. Campbell, "Microwave Signatures of First-Year and Multi-Year Sea Ice", J. Geophys. Res. 78, 3564-3572 (1973).

Gunn, K. L. S. and T. U. R. East, "The Microwave Properties of Precipitation Particles", Quart. J. Met. Soc., 80, 522-454 (1954).

Hollinger, J. P., "Passive Microwave Measurements of Sea Surface Roughness", Trans. IEEE Geoscience Electronics, GE-9, pp. 165-169 (1971).

Jackson, J. D., "Classical Electrodynamics", John Wiley & Sons, Inc., New York, (1962), p. 216ff.

Lane, J. A. and J. A. Saxton, "Dielectric Disperson in Pure Polar Liquids at Very High Radio Frequencies", Proc. Roy. Soc., London A, 214, pp. 531-545, (1952).

Nordberg, W., J. Conaway, D. B. Ross, and T. Wilheit, "Measurements of Microwave Emission from a Foam-Covered Wind Driven Sea", J. Atmos. Sci., 28, 429-435, (1971).

Rao, M. S. V., W. V. Abbott III and J. S. Theon, "Satellite-Derived Global Oceanic Rainfall Atlas" (1973 and 1974), NASA X-911-76-116, Goddard Space Flight Center, Greenbelt, Maryland (1976).

Staelin, D. A., "Measurements and Interpretation of the Microwave Spectrum of the Terrestrial Atmosphere Near 1 Centimeter Wavelength", J. Geophys., Res., 71, 2875-2881, 1966.

Staelin, D. H., A. L. Cassell, K. F. Kunzi, R. L. Pettyjohn, R. K. L. Poon, P. W. Rosenkranz, J. W. Waters, "Microwave Atmospheric Temperature Soundings: Effects of Clouds in the Nimbus-5 Satellite Data", J. Atm. Sci. 32, 1970-1976 (1975).

Waters, J. W., K. F. Kunzi, R. L. Pettyjohn, R. K. L. Poon, and D. R. Staelin, "Remote Sensing of Atmospheric Temperature Profiles with the Nimbus-5 Microwave Spectrometer", J. Atm. Sci. 32, 1953-1969 (1975).

Webster, W. J., Jr., T. T. Wilheit, D. B. Ross, and P. Gloersen, "Spectral Characteristics of the Microwave Emission from a Wind Driven Foam-Covered Sea", J. Geophys. Res. 81, 3095-3099 (1976).

Wilheit, T., "The Electrically Scanning Microwave Radiometer (ESMR) Experiment", Nimbus-5 User's Guide, NASA/Goddard Space Flight Center, Greenbelt, Maryland 59-105 (1972 I).

Wilheit, T., J. Blinn, W. Campbell, A. Edgerton, and W. Nordberg, "Aircraft Measurements of Microwave Emission from Arctic Sea Ice", Remote Sensings Environ. 2, 129-139 (1972 II).

Wilheit, T., "The Electrically Scanning Microwave Radiometer (ESMR) Experiment", Nimbus-6 User's Guide, NASA/Goddard Space Flight Center, Greenbelt, Maryland 87-108 (1975).

Wilheit, T., J. S. Theon, W. E. Shenk, L. J. Allison, and E. B. Rodgers, "Meteorological Interpretation of the Images from the Nimbus-5 Electrically Scanned Microwave Radiometer", J. App. Met. 15 166-172 (1976).

Wilheit, T., M. S. V. Rao, T. C. Chang, E. B. Rodgers, J. S. Theon, "A Satellite Technique for Quantatively Mapping Rainfall Rates over the Oceans", NASA X-911-75-72 (1975).

Wilheit, T. T., M. G. Fowler, "Microwave Radiometric Determination of Wind Speed at the Surface of the Ocean During BESEX", Joint Issue Trans. IEEE Ant. and Prop 25 111-120 (1977), and Trans. IEEE Oceanic Eng. 2 111-120 (1977).

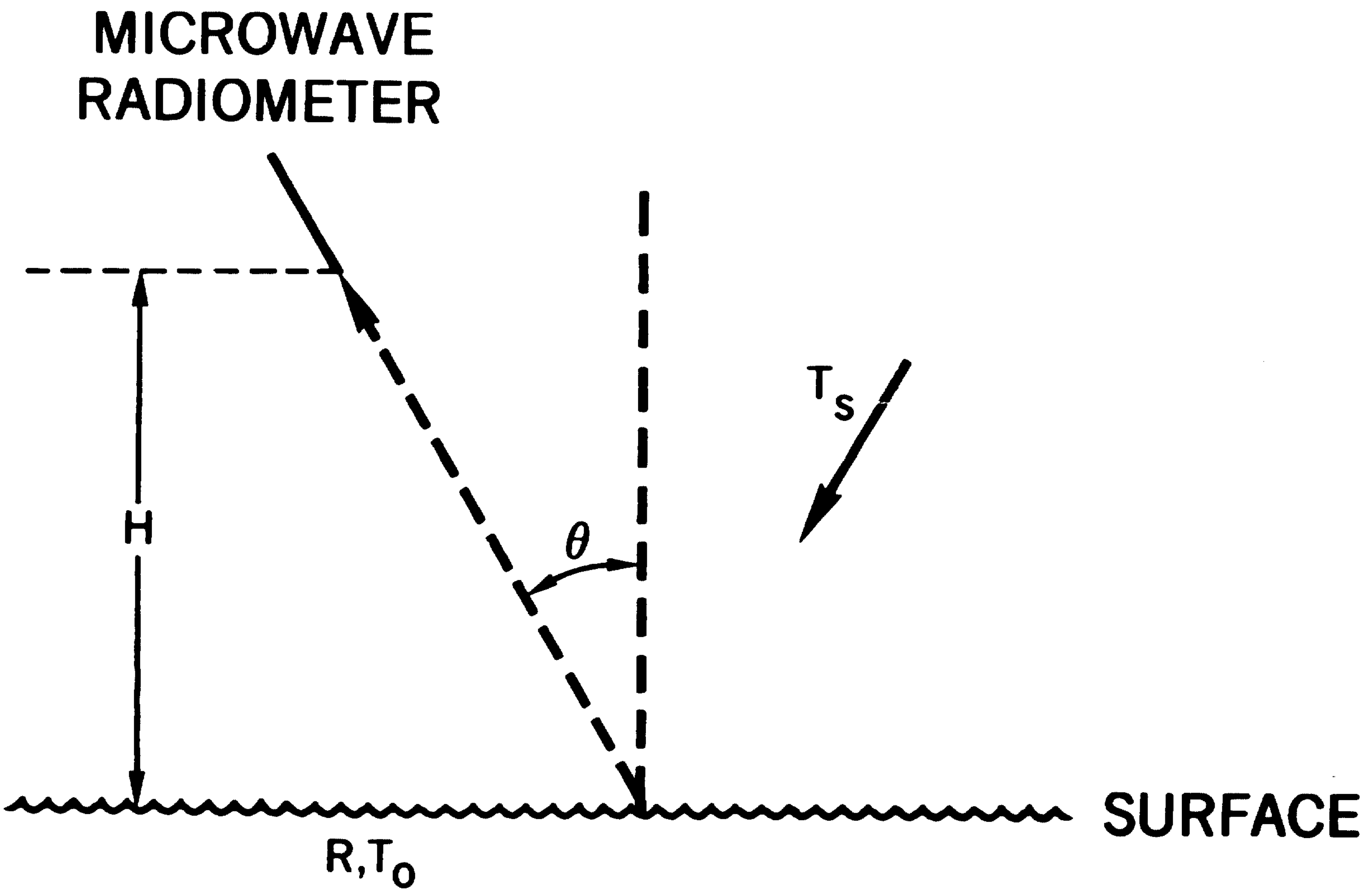

Figure 1. Typical Viewing Geometry for Microwave Remote Sensing of Ocean Surface and Atmosphere

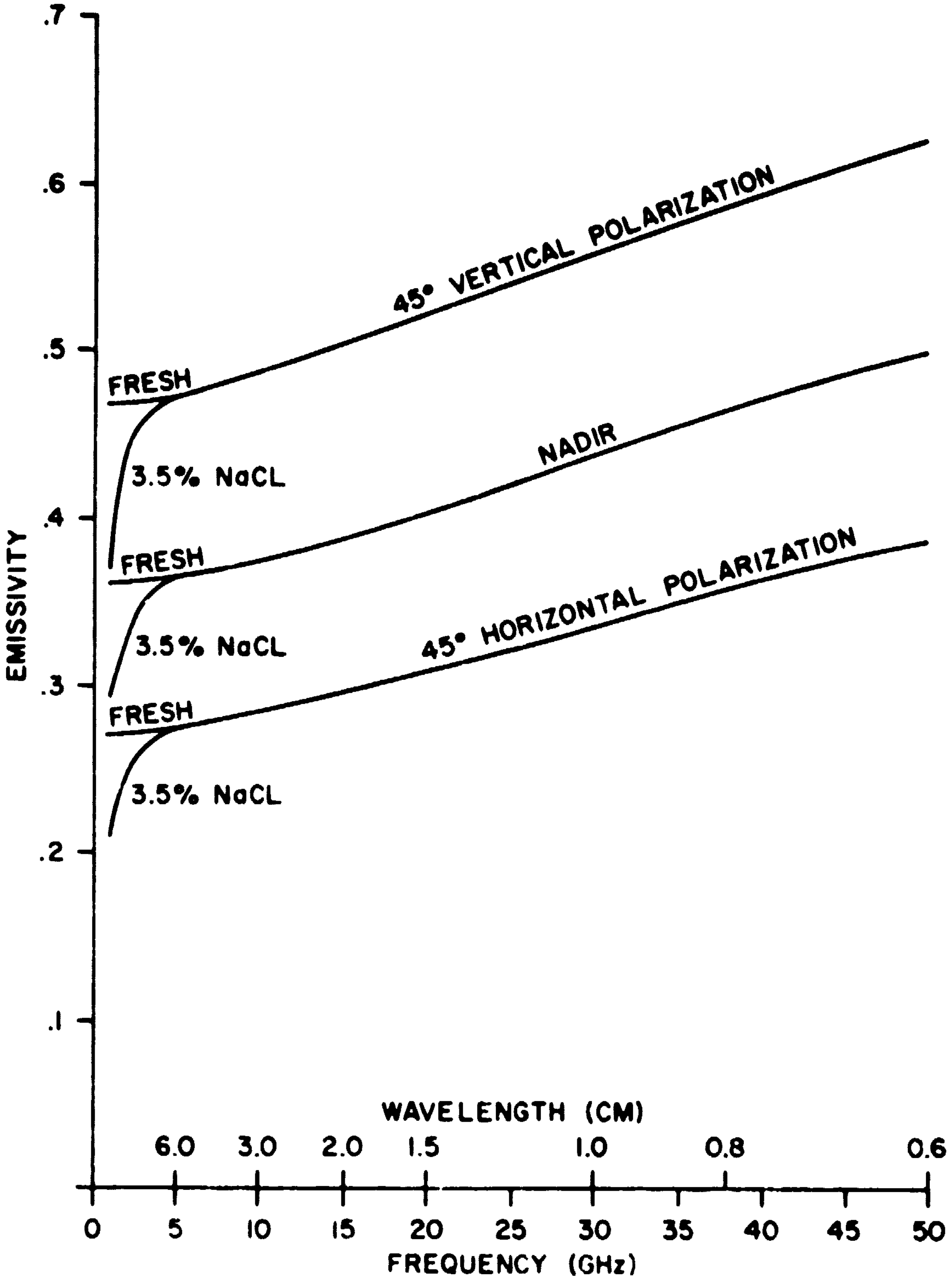

Figure 2. Emissivity of Smooth Water Surface at 20°C

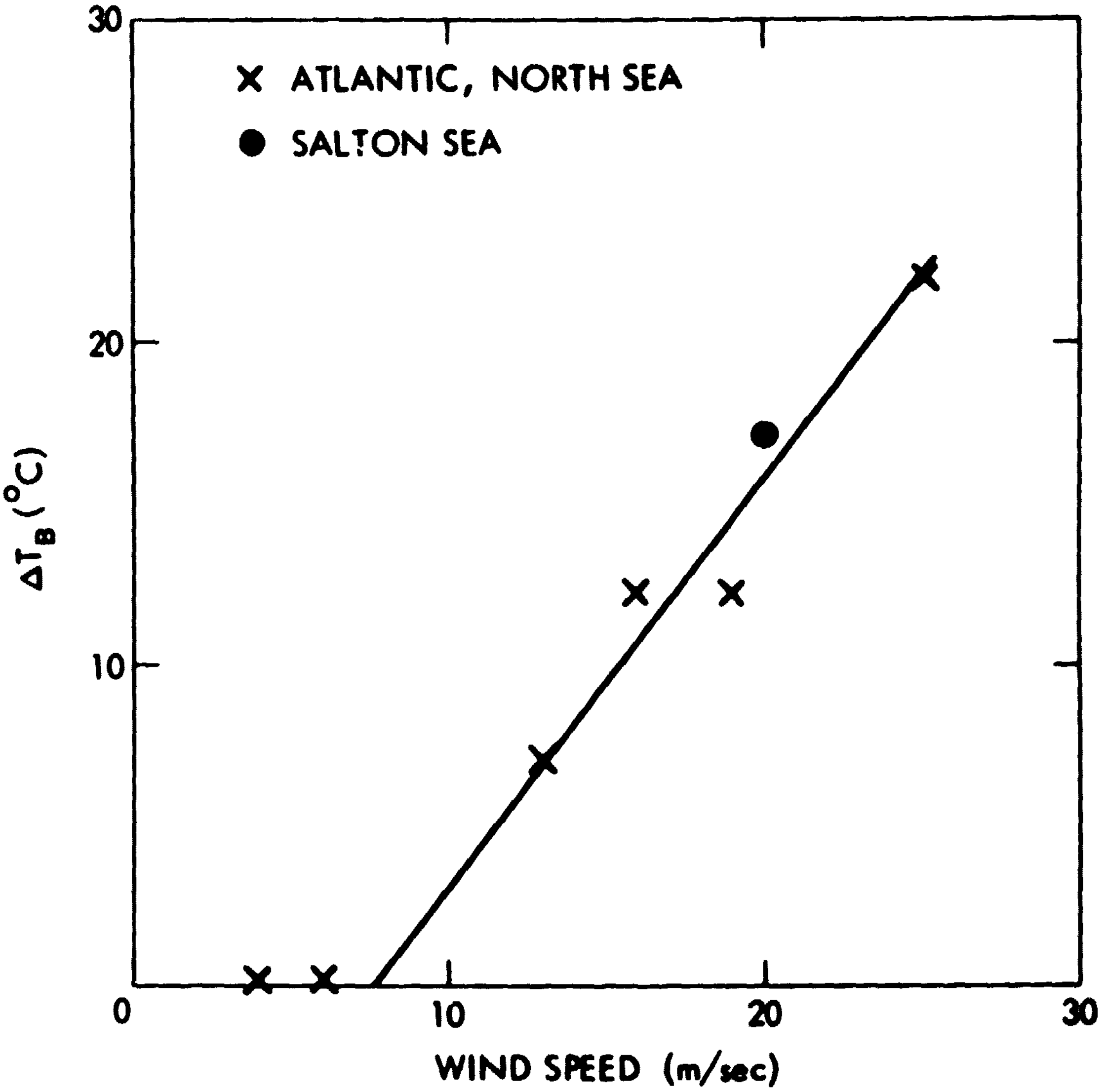

Figure 3. Increase of Brightness Temperature at 19.35 GHz Caused by Wind Speed at the Ocean Surface

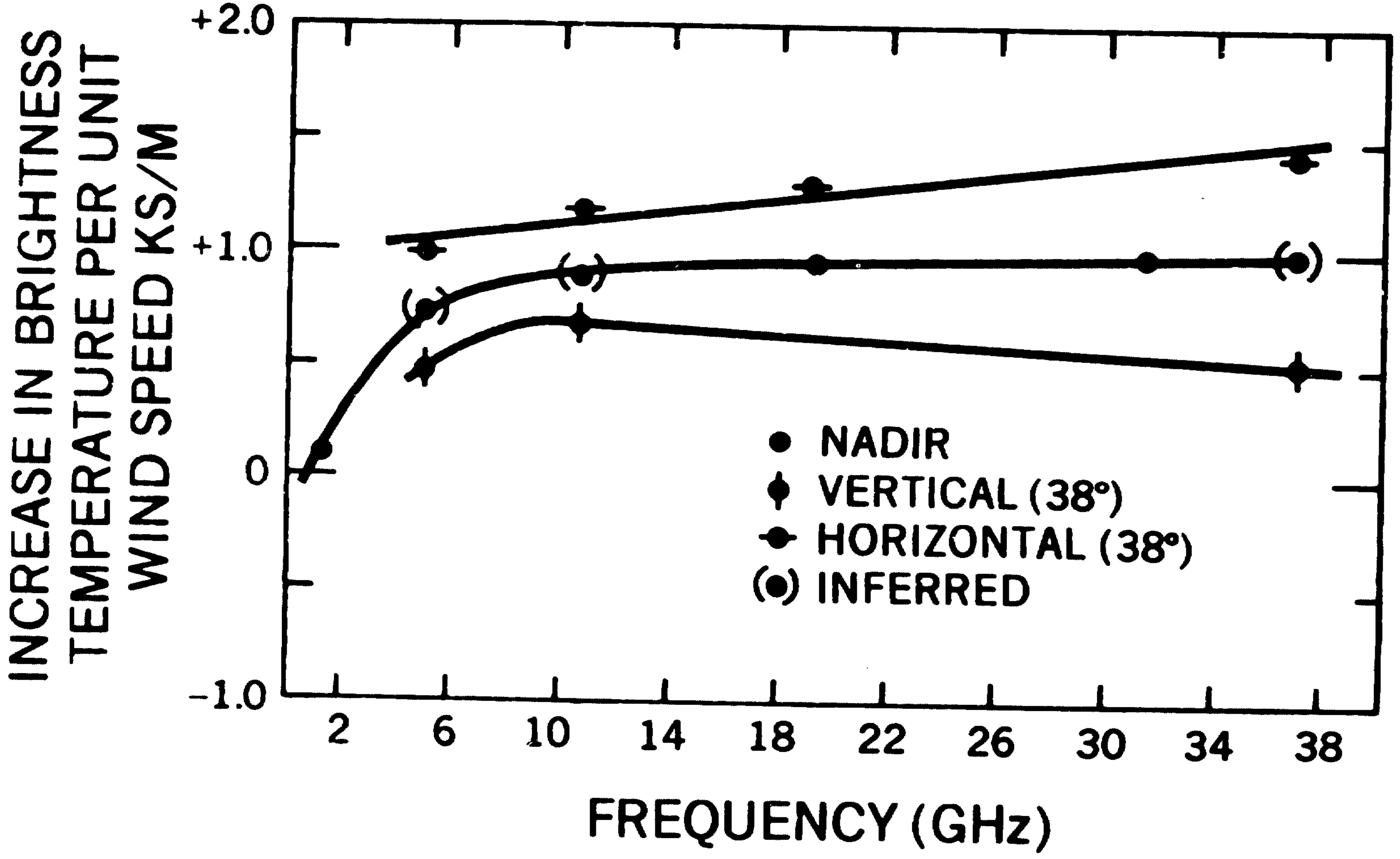

Figure 4. Rate of Increase of Brightness Temperature with Wind Speed as a Function of Frequency

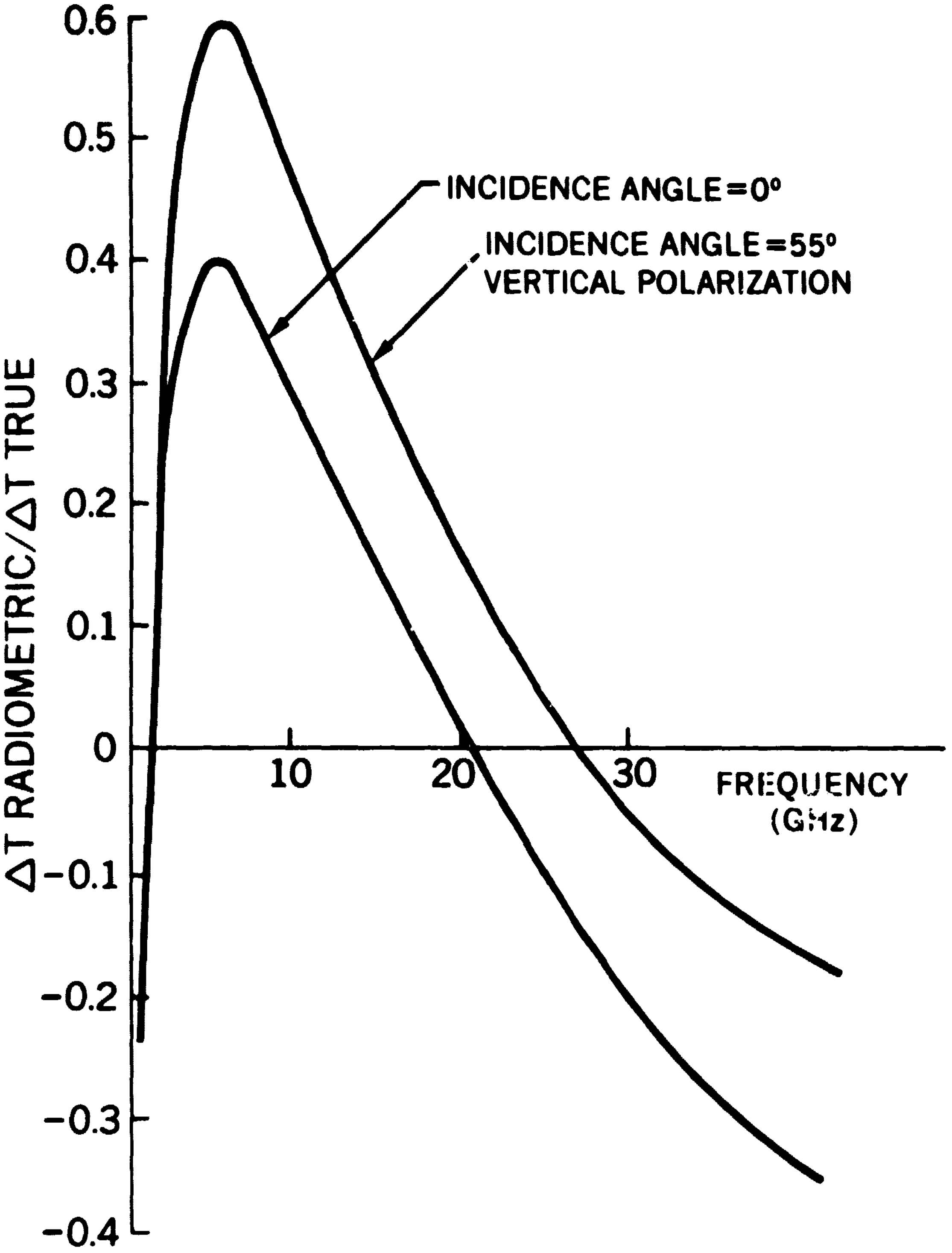

Figure 5. Sensitivity of Microwave Brightness Temperature to Sea Surface Thermodynamic Temperature over the Range 0 to 30°C

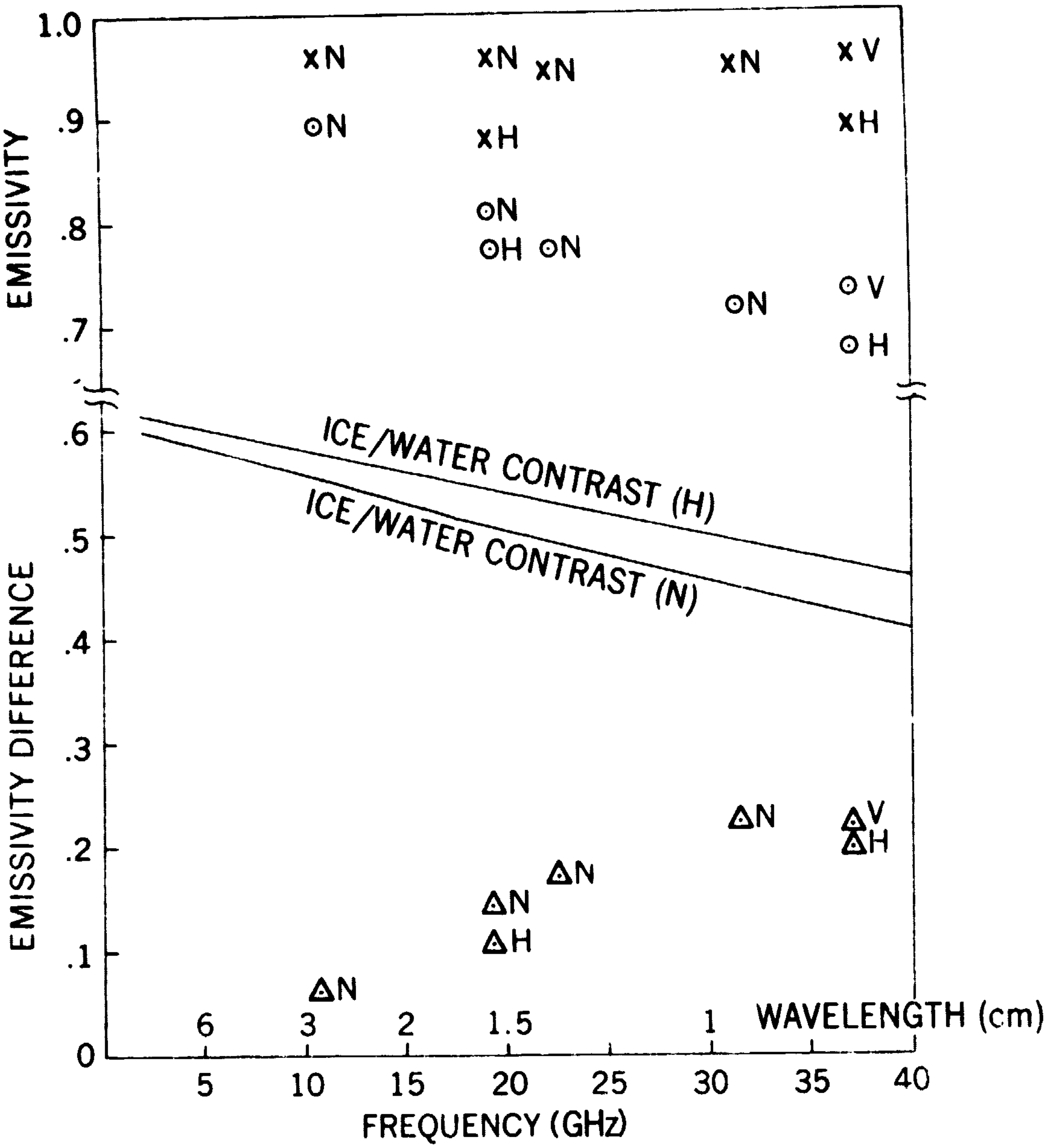

Figure 6. Emissivity of First Year (New) and Multi-Year (Old) Sea Ice: N - Nadir Viewing; H - Viewing 45° Left of Nadir—Horizontal Polarization; V - Viewing 45° Left of Nadir—Vertical Polarization; X - "New" Ice; ʘ - "Old" Ice; Δ - ε (New)—ε (Old)

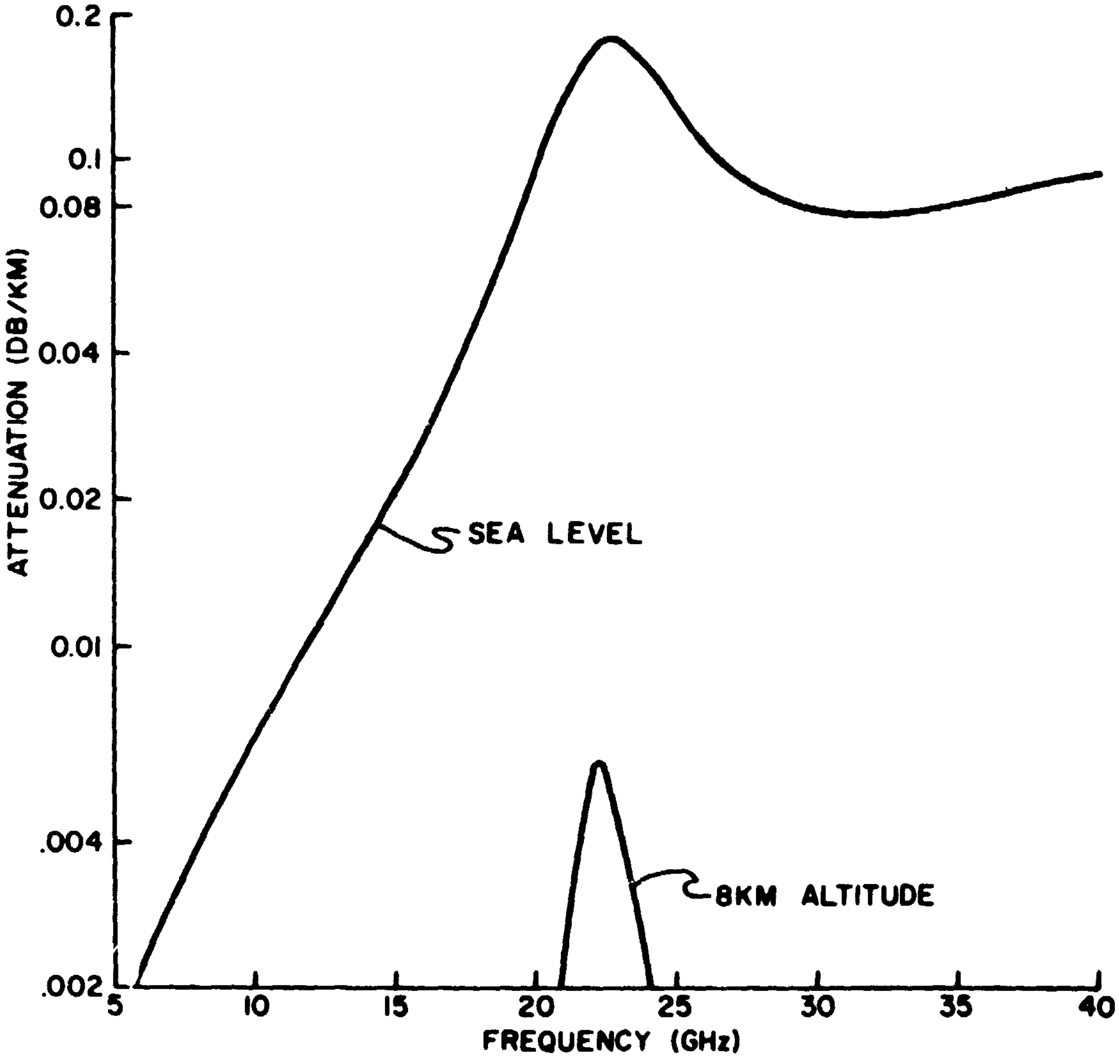

Figure 7. Microwave Attenuation due to Atmospheric Water Vapor - 1962 United States Standard Atmosphere

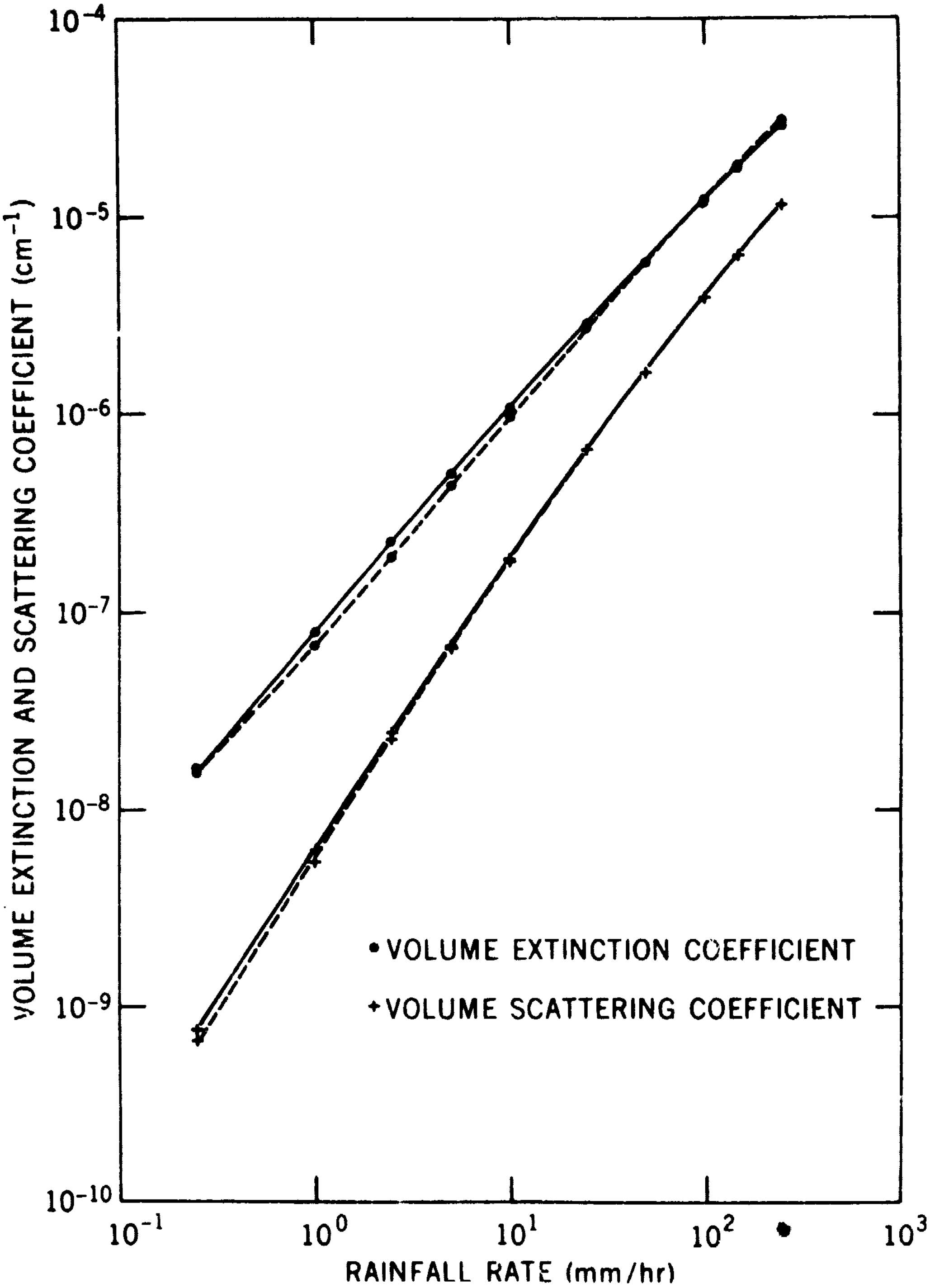

Figure 8. Scattering and Extinction (Absorption + Scattering) by Rain at 19.35 GHz. The solid and dashed lines represent temperatures of 20 and 0°C respectively.

NIMBUS-5
ESMR
JANUARY 22, 1973

Figure 9. Nimbus-5 ESMR Image Showing Rain Feature Crossing Florida. The dynamic range of the image is from approximately 190 K (light) to 250 K (dark).

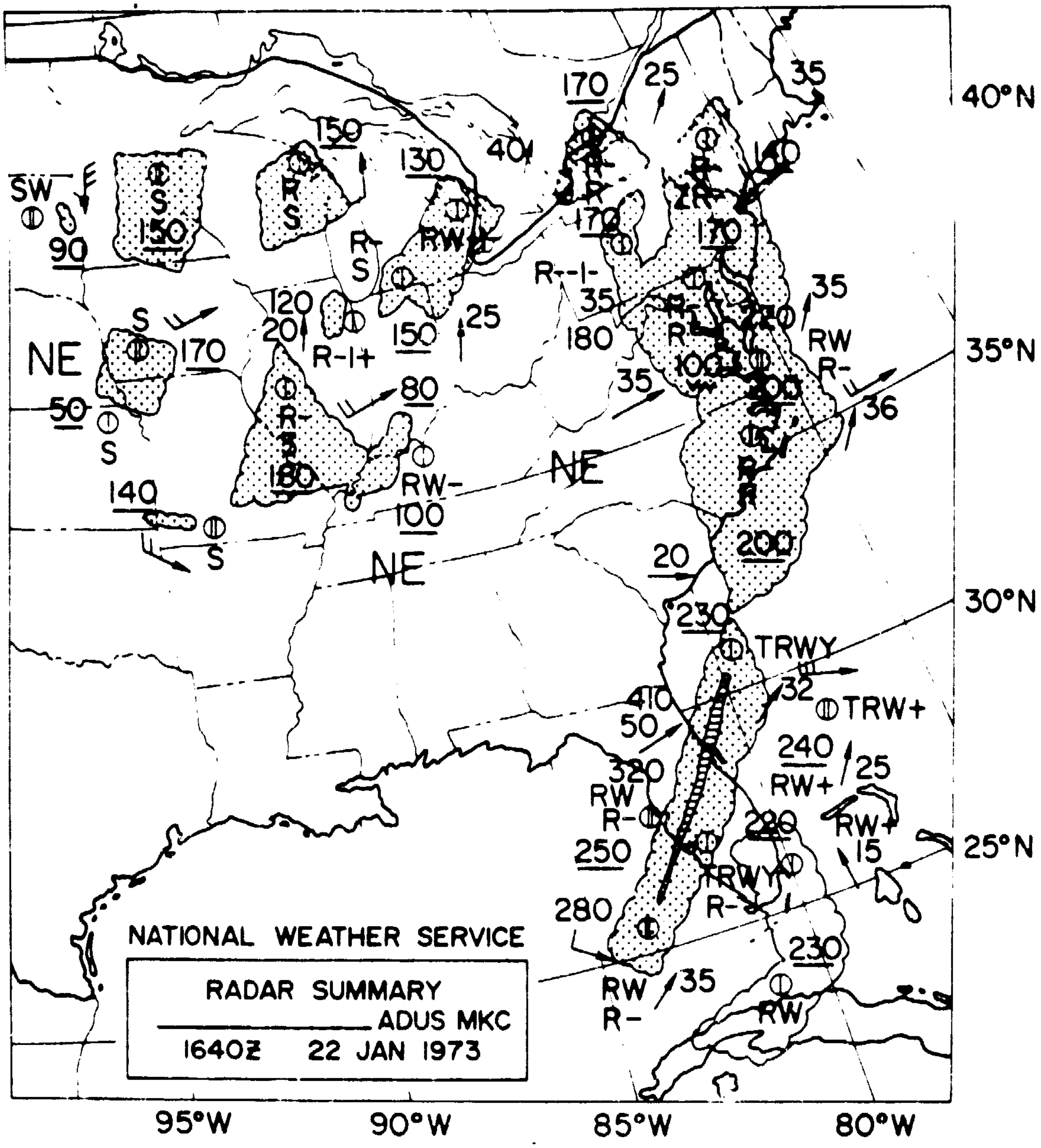

Figure 10. Radar (Rain Area) Summary Corresponding to Figure 9

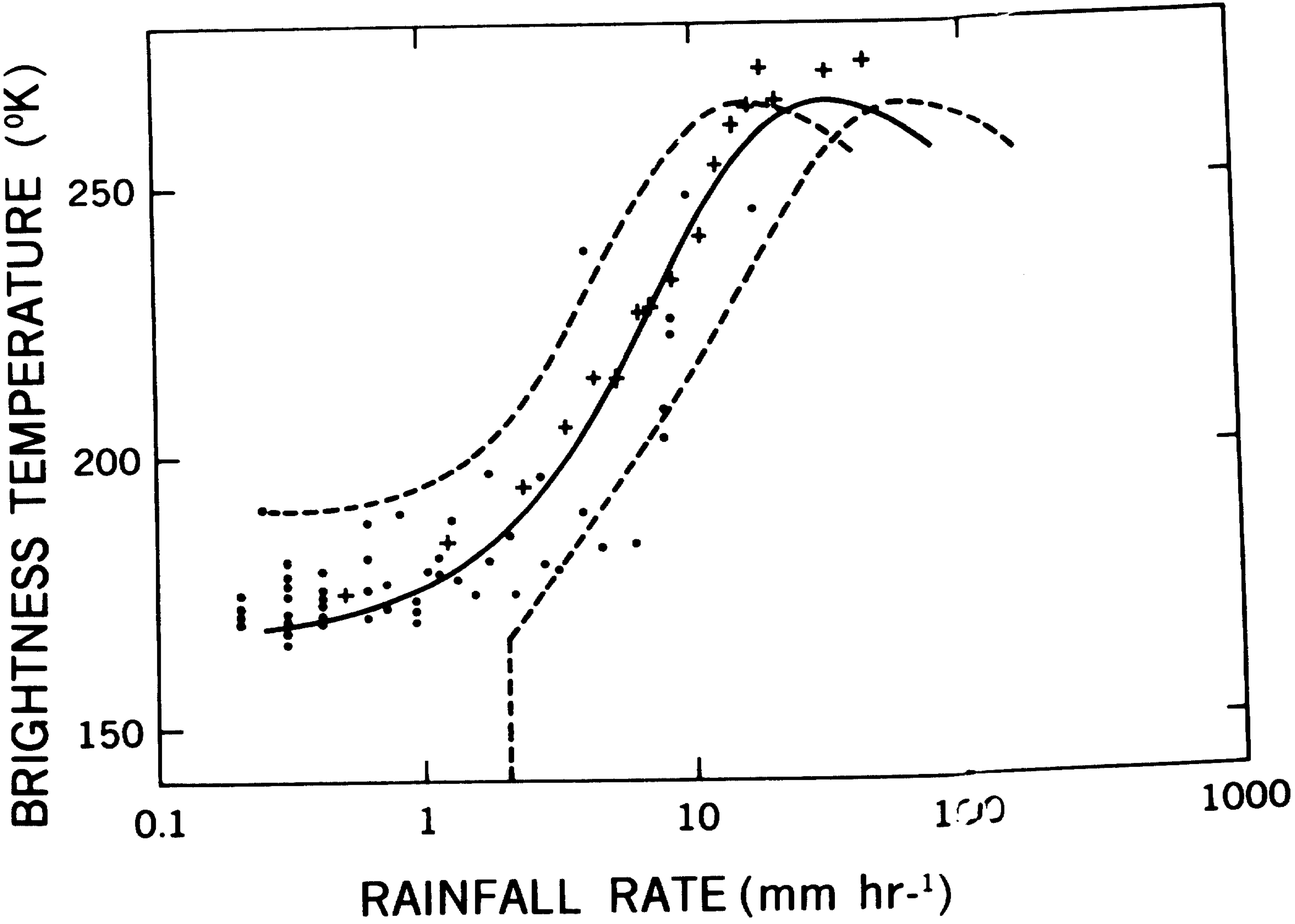

Figure 11. Brightness Temperature at 19.35 GHz as a Function of Rain Rate over the Ocean

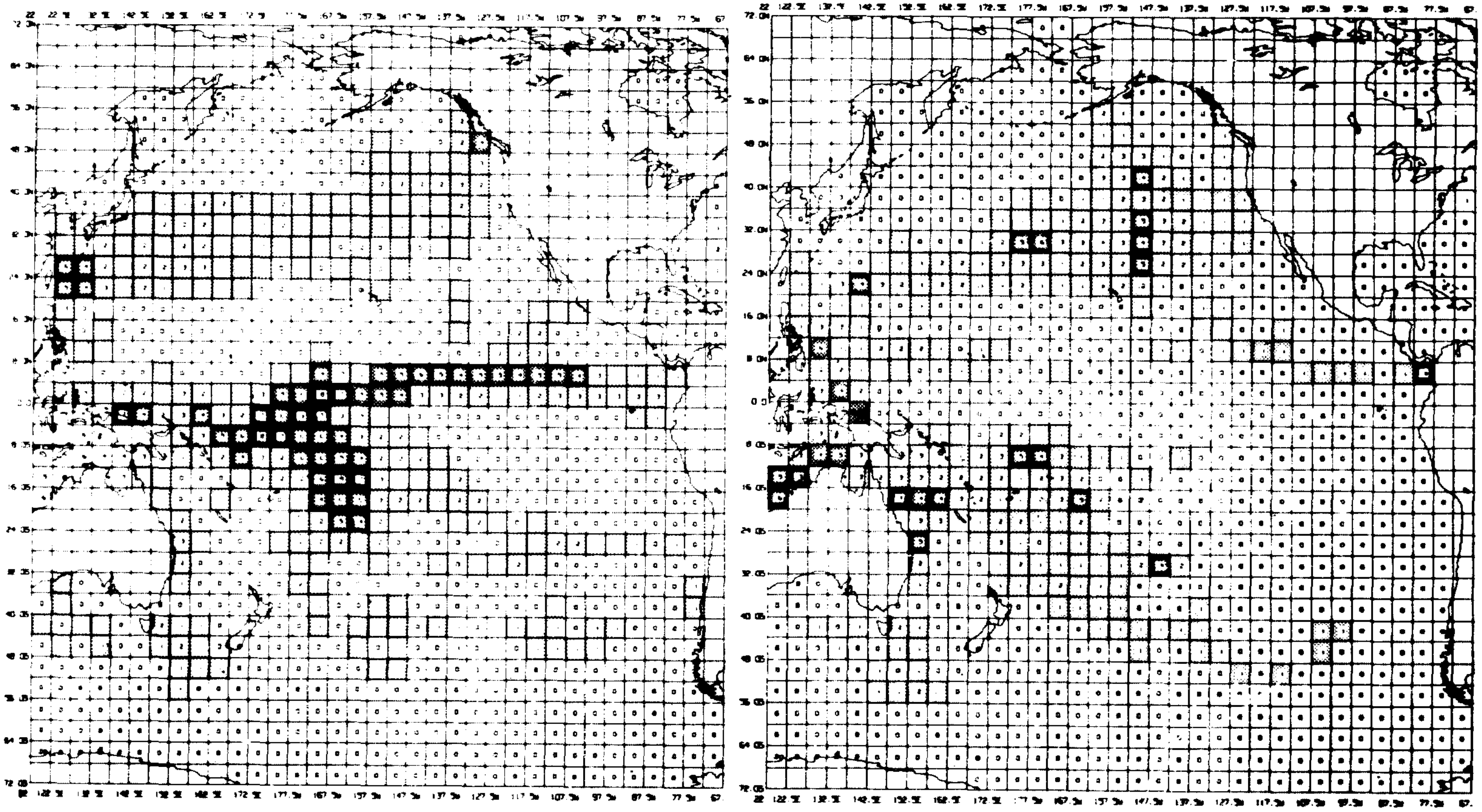

Figure 12. Nimbus-5 ESMR Derived Rainfall Maps for January 1973 (El Niño Year) and January 1974 (Non-El Niño Year)

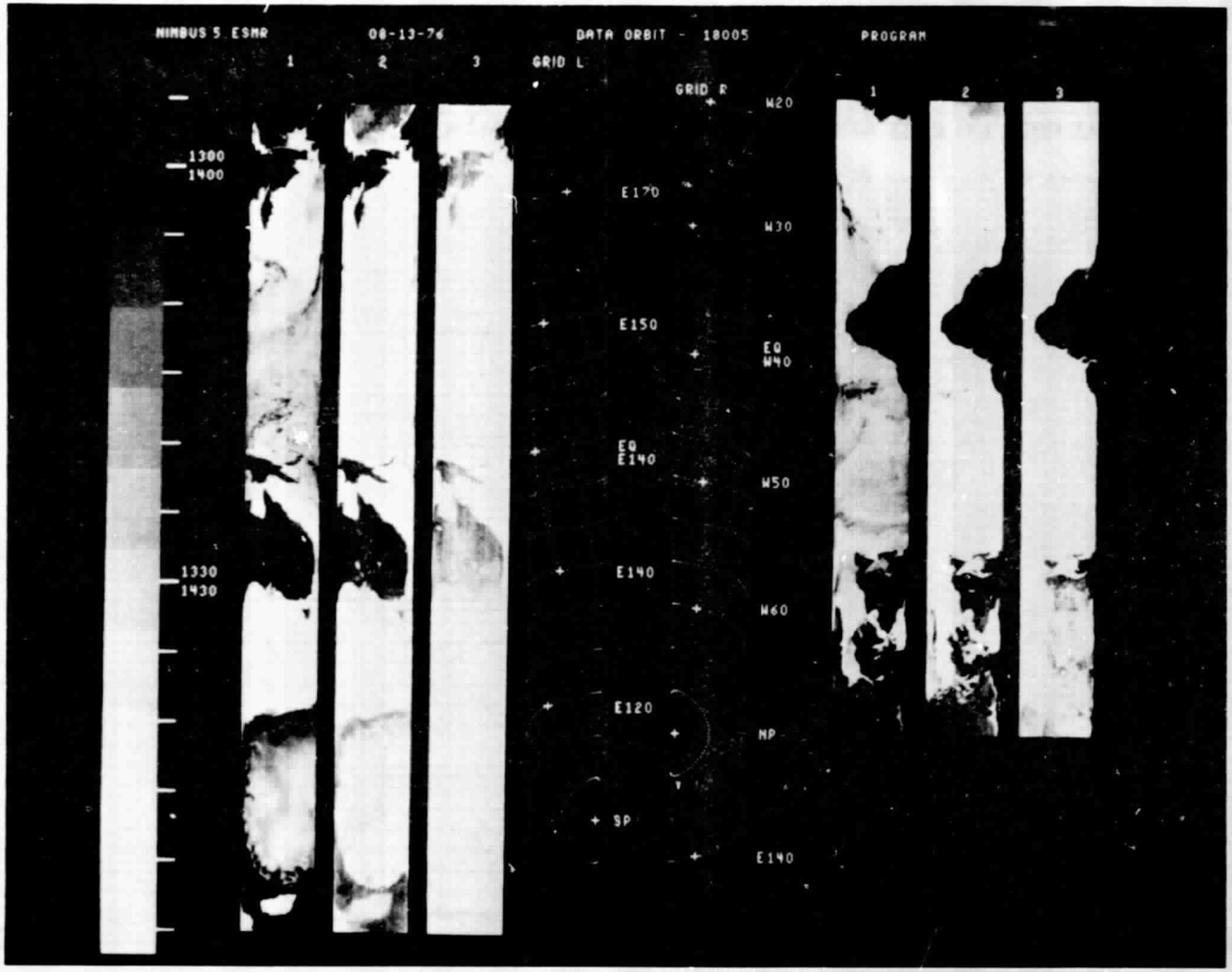

Figure 13. Typical Nimbus-5 ESMR Data Product Used by the U.S. Navy for Sea Ice Analysis

FIGURE CAPTIONS

Figure 1. Typical Viewing Geometry for Microwave Remote Sensing of Ocean Surface and Atmosphere

Figure 2. Emissivity of Smooth Water Surface at 20° C

Figure 3. Increase of Brightness Temperature at 19.35 GHz Caused by Wind Speed at the Ocean Surface

Figure 4. Rate of Increase of Brightness Temperature with Wind Speed as a Function of Frequency

Figure 5. Sensitivity of Microwave Brightness Temperature to Sea Surface Thermodynamic Temperature over the Range 0 to 30° C

Figure 6. Emissivity of First Year (New) and Multi-Year (Old) Sea Ice: N - Nadir Viewing; H - Viewing 45° Left of Nadir—Horizontal Polarization; V - Viewing 45° Left of Nadir—Vertical Polarization; X - "New" Ice; ⊙ - "Old" Ice; △ - ϵ (New)—ϵ (Old)

Figure 7. Microwave Attenuation due to Atmospheric Water Vapor - 1962 United States Standard Atmosphere

Figure 8. Scattering and Extinction (Absorption + Scattering) by Rain at 19.35 GHz. The solid and dashed lines represent temperatures of 20 and 0° C respectively.

FIGURE CAPTIONS (Continued)

Figure 9. Nimbus-5 ESMR Image Showing Rain Feature Crossing Florida. The dynamic range of the image is from approximately 190 K (light) to 250 K (dark).

Figure 10. Radar (Rain Area) Summary Corresponding to Figure 9

Figure 11. Brightness Temperature at 19.35 GHz as a Function of Rain Rate over the Ocean

Figure 12. Nimbus-5 ESMR Derived Rainfall Maps for January 1973 (El Niño Year) and January 1974 (Non-El Niño Year)

Figure 13. Typical Nimbus-5 ESMR Data Product Used by the U.S. Navy for Sea Ice Analysis